

## Healthier routes planning: A new method and online implementation for minimizing air pollution exposure risk



Bin Zou<sup>a,\*</sup>, Shenxin Li<sup>a</sup>, Zhong Zheng<sup>b</sup>, Benjamin F. Zhan<sup>c</sup>, Zhonglin Yang<sup>a</sup>, Neng Wan<sup>d</sup>

<sup>a</sup> School of Geosciences and Info-Physics, Central South University, Changsha 410083, China

<sup>b</sup> College of Resources and Environment, Chengdu University of Information Technology, Chengdu 610225, China

<sup>c</sup> Department of Geography, Texas State University, San Marcos, TX 78666, USA

<sup>d</sup> Department of Geography, University of Utah, Salt Lake City, UT 84112, USA

### ARTICLE INFO

#### Keywords:

Air pollution mapping  
Route planning  
Exposure risk assessment  
Land use regression

### ABSTRACT

Air pollution exposure during daily traveling is growing as an increasingly serious factor affecting public health with rapid incensement of travel distance in urban sprawl. Finding a healthier route with least exposure risk might be an alternative way to mitigate adverse health outcomes under the truth that worldwide air pollution in urban area cannot be eliminated within a short period of time. Integrating techniques of fine scale mapping of air pollutant concentration, risk weight estimation of road segment exposure to air pollutants, and dynamic Dijkstra algorithm capable of updating route, this study for the first time proposes a healthier route planning (HRP) method to minimize personal travel exposure risk to air pollution. Effectiveness of HRP in mitigating exposure risk was systematically tested based on hundred pairs of origins and destinations located in Beijing-Tianjin-Hebei (BTH) of China with necessarily dense air quality observations. Results show that the spatiotemporal variations of air pollutant concentrations were significant and these differences indeed occurred with time at hourly scale. Meanwhile, the grid-based estimation of exposure risk is time dependent with risk ranging from 5 to 109, which echoes the necessity of healthier route planning. Compared to routes with the shortest distance and least travel time, healthier route has the least exposure risk. And this risk mitigation effect is more significant in areas with wide exposure risk variations than those in areas without obvious risk difference over space (e.g., 21.38% vs. 0.86%). Results suggest that HRP method is promising to minimize personal exposure risk during daily travel based on the accurate exposure risk estimation of road segment at high spatiotemporal resolution. This role could be more important in areas with longer travel distance and greater heterogeneous distribution of air pollution in great metropolis.

### 1. Introduction

Personal travel is intimately bound up with the progress of human society and its behavior choice is always faced in daily life (Fu & Lam, 2014). In the traditional process of route choosing, the shorter distance route (Choi, Kang, & Bahk, 2014), the less travel time (George & Kim, 2013), the better road condition (Paul, 2013; Ramezani & Geroliminis, 2012), and the cheaper money cost (Rahmani & Koutsopoulos, 2013) generally are primary considerations. However, these considerations are not sufficient since air pollution, one of the most serious environment problems nowadays, affects public health during traveling time (Scott et al., 2011). In terms of possibility in mitigating adverse health effect during personal traveling time, there is an urgent need to lower the air pollution exposure (APE) risk for a person through detecting the best route to travel (Schepers, Fishman, Beelen, et al., 2015).

Specifically, a growing number of people are concerned about the adverse health effect in recent years with the rapid economy development and the improvement of living standards (Zheng & Kahn, 2013; Zou, You, & Lin, 2019). Moreover, these concerns are particularly significant for susceptible population due to the increasing daily travel time with longer travel distance in large urban areas (Hynes, 2013). The greater APE risk caused by increasing traveling time is placing more serious stress on those susceptible people than ever before (Guarnieri & Balmes, 2014). What is more, worldwide air pollutant emissions will not drop dramatically in a short period, which makes air pollution exposure a consistent health risk in the next decade. Therefore, reasonable circumvention of personal APE risk is becoming an alternatively promising way to protecting human health.

Some previous studies (, , , , Alexiou & Katsavounis, 2015, Bigazzi & Figliozzi, 2015, Mölter & Lindley, 2015, Sharker & Karimi, 2014)

\* Corresponding author at: No. 932, South Lushan Road, Yuelu District, Changsha City 410083, China.

E-mail address: [210010@csu.edu.cn](mailto:210010@csu.edu.cn) (B. Zou).

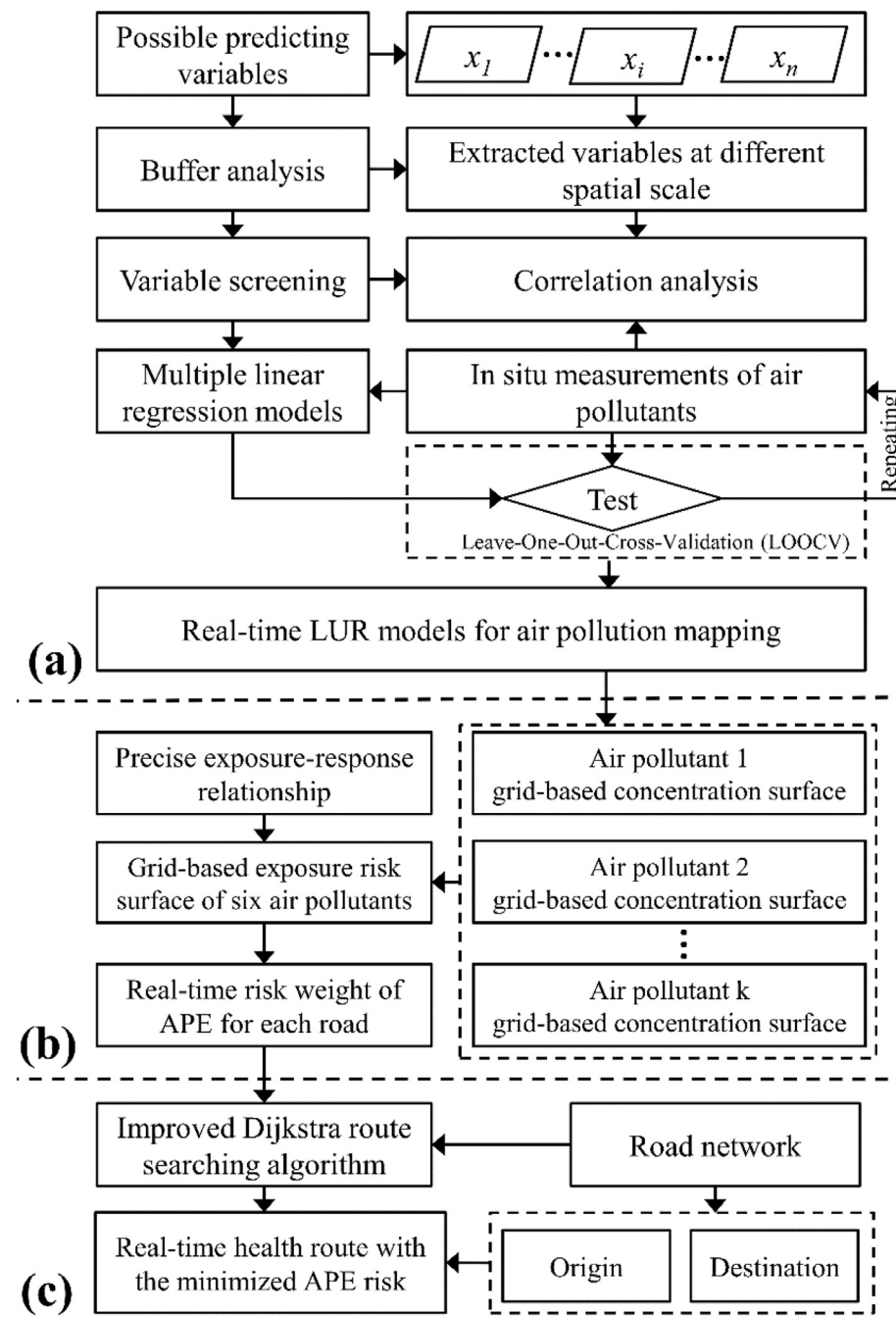


Fig. 1. The flowchart of near real-time healthier route search method.

have introduced the idea of least air pollution exposure by calculated through steps including a distance interval-fixed resampling of road segments, spatially continuous surface of air quality index (AQI) interpolated by discrete values at stationary monitoring sites, and static route search with traditional methods introduced by Dijkstra (1959). However, APE risk at a road segment not only depends on the air pollutant concentration-based exposure intensity but also relates to the pollutant-based adverse health effects (Zou, Zheng, Wan, et al., 2016). Consequently, variations of APE risk among road segments along a road depends on the heterogeneous distribution of air pollutant concentration based adverse health effects. This is a core concept obviously different from the previous method that only focuses on the comparison of APE intensities among road segments, rather than potential adverse health effects (i.e. APE risk titled in this study) based on the real exposure-response parameters (Ezzati & Kammen, 2001; Lelieveld, Evans, Fnais, et al., 2015; Shang, Sun, Cao, et al., 2013).

More importantly, the prerequisite of accurate calculation of present study is the fine scale (i.e. higher spatiotemporal resolution) continuous surface of air pollutant concentration. While the present method directly uses inverse distance weighted (IDW) and ordinary kriging (OK) to compensate the deficiency of stationary point measured AQI, these simple interpolation methods are usually too rough to produce the continuous surface at adequate spatial resolution under the currently sparse monitoring network (Jerrett, Arain, Kanaroglou, et al., 2005; Zou, Luo, Wan, et al., 2015). Meanwhile, although the AQI is a widely used index indicating the health level of air quality (Airnow Website, 2015, U.S. Environmental Protection Agency 2014), it cannot veritably depict the air pollution exposure risk comprehensively caused by various air pollutants with certain adverse health effects (e.g., mortality rate) (Pope, Burnett, Krewski, et al., 2009). In other words, the previous

method suffered from the lack of consideration of the precise exposure-response relationship between the potential air pollutants and corresponding health endpoints (Franklin, Zeka, & Schwartz, 2007; Pope et al., 2009). Additionally, the static least exposure route searched by previous method is impractical because it may vary with the change of spatial distribution pattern of air pollutant concentration over space and time and this could indeed happen with the gradually longer travel distance or time between origins and destinations in large urban areas.

Nevertheless, technological revolutions and new research findings are gradually emerging as possible solutions to the above inadequacies. Typically, multi-factor based regression modeling, including land use regression (LUR) and geographical weighted regression (GWR), has been proven as reliable methods for fine scale air pollution mapping (Zou, Pu, Bilal, et al., 2016). By fusing the aerosol optical depth (AOD), land use cover, meteorological factors, traffic and terrain, LUR and GWR modeling can produce the continuous surface of air pollutant concentration with sparse ground monitoring data as inputs (Zou et al., 2015; Hoek, Beelen, Hoogh, et al., 2008; Xu, Zou, Lin, et al., 2019). Synchronously, widely accepted exposure response relationships have been revealed for major air pollutants (e.g., PM<sub>2.5</sub>) through global and local panel studies of air pollutant related chronic adverse health effects (Lelieveld et al., 2015; Shang et al., 2013). Meanwhile, ideas of dynamically updating searched routes by adding the real-time traffic jam information was realized recently (Choi et al., 2014; Qian & Zhang, 2013; Pillac, Gendreau, Guéret, et al., 2013; Mainali, Mabu, Yu, et al., 2011), and this actually offers a success background to improve the static least exposure route search method to a dynamic one through fusing real time information of adverse health effects caused by air pollutant concentration at fine scale.

The ultimate goal of this study is to develop a new near real-time healthier route planning (HRP) method and an experimental online implementation service to minimize public APE risk in daily travel by validating the HRP method's feasibility and reliability in a case study. The entire study mainly concentrates on the HRP method with steps including the fine scale mapping of air pollutant concentration, risk weight estimation of road segment exposure to air pollutants, dynamic updating mechanism of the Dijkstra algorithm in healthier route search, as well as the development of experimental online implementation service. As a result, the HRP method would be a boost in healthier route planning through the achievement of fine scale APE risk estimation in real time with above steps, and will provide a way to minimize exposure risk and protect human health through improved travel behaviors.

## 2. HRP method and online implementation service

Based on the risk assessment procedure of air pollution exposure, the integrated HRP method theoretically consists of three steps as listed in Fig. 1. (a) fine scale mapping of air pollutant concentration; (b) risk weight calculation of APE for each road; (c) near real-time healthier route search. The detail description of each step is shown as follow.

### 2.1. Fine scale mapping of air pollutant concentration

As shown in Fig. 1, the first step of accurately estimating APE risk is the continuous surface mapping of air pollutant concentrations. In light of the good reputation of LUR modeling (Jerrett, Arain, Kanaroglou, et al., 2007; Olvera et al., 2012), the air quality data, AOD data, road network and surface dust data, meteorological data, as well as other ancillary data could be collected to develop the real-time LUR models.

The structure of regression modeling can be defined as follows:

$$y = \alpha_0 + \alpha_1 x_1 + \alpha_2 x_2 + \dots + \alpha_n x_n + u$$

where  $y$  is the estimation of the hourly average air pollutant concentration,  $x_1, x_2, \dots, x_n$  are independent variables,  $\alpha_0$  is a constant,  $\alpha_1, \alpha_2, \dots, \alpha_n$  are regression coefficients for each predictor, and  $u$  is the

random error.

This process can be implemented by variable screening, multi-linear regression modeling, and model validation. Subsequently, based on the developed models, continuous surfaces of air pollutant concentrations with 500 m's resolution can be created. As a result, the optimal hourly LUR models were determined based on the model performance indicators (fitting  $R^2$ , RMSE) computed by the Leave-One-Out-Cross-Validation (LOOCV) technique (Johnson, Isakov, Touma, et al., 2010). The calculations of  $R^2$  and RMSE are as following equations.

$$R^2 = \frac{\sum_{i=1}^n (y'_i - \bar{y}_i)^2}{\sum_{i=1}^n (y_i - \bar{y}_i)^2} \quad (1)$$

$$RMSE = \sqrt{\frac{1}{n} \sum_{i=1}^n (y_i - y'_i)^2} \quad (2)$$

where,  $y_i$  represents observations,  $y'_i$  is the predicted value of  $y_i$ ,  $\bar{y}_i$  represents the average value of  $y_i$ ,  $n$  is the number of samples.

### 2.2. Calculations of APE risk weight for each road

Scientific evidence suggests that traveling along a road may cause various levels of hazardous health outcomes due to exposure to air pollutants (Stutzer & Frey, 2008), especially for children (Hajat, Armstrong, Wilkinson, et al., 2007; Ritz, Wilhelm, & Zhao, 2006) and this is especially true to pregnant women (Faiz, Rhoads, Demissie, et al., 2012; Defranco, Hall, Hossain, et al., 2015). Thus, the APE risk weight of HRP for a road can be calculated through the road segment-based exposure risk estimation, and the exposure risk accumulation of all road segments of a road.

Considering the exposure-response parameters and the grid-based concentration maps of air pollutants with higher spatiotemporal resolution, the grid-based APE risk associated with road segments can be first computed using formula (3) given below:

$$R_{i,j}^{m,t} = \frac{\sum_{k=1}^n \left( M^k * \frac{1}{10} * (C_{i,j}^{k,m,t} - C_0^k) \right)}{M} \quad (3)$$

where  $R_{i,j}^{m,t}$  is the exposure risk coefficient of grid cell  $(i,j)$  covering road  $m$  at time  $t$ ,  $M^k$  is the rising mortality rate of air pollutant  $k$  under per 10  $\mu\text{g}/\text{m}^3$  increment (note:  $M^1, M^2, M^3, M^4, M^5$  and  $M^6$  indicate the mortality rates of PM<sub>2.5</sub>, PM<sub>10</sub>, SO<sub>2</sub>, CO, NO<sub>2</sub>, and O<sub>3</sub>, respectively),  $C_{i,j}^{k,m,t}$  is the concentration of air pollutant  $k$  at grid cell  $(i,j)$  at time  $t$ , and  $C_0^k$  represents the threshold of risk-exposure associated with air pollutant  $k$  (see Table 1),  $M$  is a constant (the value is 3.43%, the sum of six pollutant's mortality rate according to table1).

Second, by overlaying the road network with the grid-based APE risk surface, length of the road segment located in each grid can be extracted. Along with the road segment in each grid cell, the traveling time (i.e. time needed to pass through this road segment) can be

**Table 1**

Exposure-response parameters of air pollutants for adverse health effect assessment.

Air pollutants	Rising mortality rate <sup>a</sup>	Threshold for risky exposure ( $\mu\text{g}/\text{m}^3$ ) <sup>b</sup>
PM <sub>2.5</sub>	0.40%	25
PM <sub>10</sub>	0.31%	50
NO <sub>2</sub>	1.40%	200
SO <sub>2</sub>	0.71%	20
O <sub>3</sub>	0.42%	100
CO	0.19%	30 <sup>d</sup>

<sup>a</sup> Means the mortality risk rises with an increase of air pollutant concentrations (Lai, Tsang, & Wong, 2013; Lu, Xu, Cheng, et al., 2015; Wang, Wang, & Bai, 2012).

<sup>b</sup> Threshold for risky exposure based on WHO's recommended Air Quality Guidelines for common air pollutants.

calculated with the speed and congestion information of road to which that road segment belongs. After completing the above-mentioned procedures, the risk weight of APE for each road segment of a road  $m$  can be measured as formula (4):

$$W_{i,j}^{m,t} = \frac{d_{i,j}^m}{(V^m * \delta^m)} * R_{i,j}^{m,t} \quad (4)$$

where  $W_{i,j}^{m,t}$  denotes the risk weight of APE at time  $t$  for a road  $m$  covered by grid cell  $(i,j)$ ,  $V^m$  denotes the speed limit of the road  $m$ ,  $d_{i,j}^m$  is the length of the road  $m$ 's segment located in grid cell  $(i,j)$ , and  $\delta^m$  is a congestion factor which is useful for exposure time emendation in computing the risk weight of APE.

Finally, the risk weight of APE for road  $m$  in the road network can be integrated by formula (5):

$$W^{m,t} = \sum_{i=1,j=1} W_{i,j}^{m,t} \quad (5)$$

where  $W^{m,t}$  is the risk weight of APE for road  $m$  at time  $t$  and this process can be simply repeated to compute the risk weight of APE for all the roads covered by the grid-based exposure risk surface.

### 2.3. Near real-time healthier route search

Before the route search, the road data was converted to network dataset after the process of setting network source, setting network dataset, and creating network dataset. Then, a dynamic Dijkstra

algorithm can be employed to determine the near real-time healthier route with the lowest risk weight of APE dynamically (see Fig. 2). At this stage, the dynamic Dijkstra algorithm could identify the healthier route with the lowest risk accumulative weight of APE from the start vertex (i.e. initialized as the origin) to every other vertex step by step. As described in Fig. 2, each vertex within the digraph will be spanned repeatedly. When all the vertices have been marked, the union of these sequenced vertices along the route from the start vertex to the last marked vertices is defined as the final healthier route. Meanwhile, it should be noted that the dynamic Dijkstra route can update the healthier route automatically base on dynamical data. This automatic update does usually happen when the travel time spans than one hour and data are updated hourly.

At start time  $t$ , for all roads (their number is  $u$ ) along the determined healthier route ( $r$ ), suppose the total length is  $S^r$  and the traveling speed is  $V^r$ , the total time  $\Delta t$  for passing the roads can thus be estimated as follow:

$$\Delta t = \sum_{r=1}^u \frac{S^r}{V^r} \quad (6)$$

When the air pollution concentrations at a certain instant between the start time (i.e.,  $t$ ) and the estimated arriving time (i.e.,  $t + \Delta t$ ) spatially varies compared to the one employed for computing the risk weight of APE at start time  $t$ , the dynamic Dijkstra route search algorithm will automatically start the updating process. In this process, roads not passed before this update with the lowest risk weight of APE

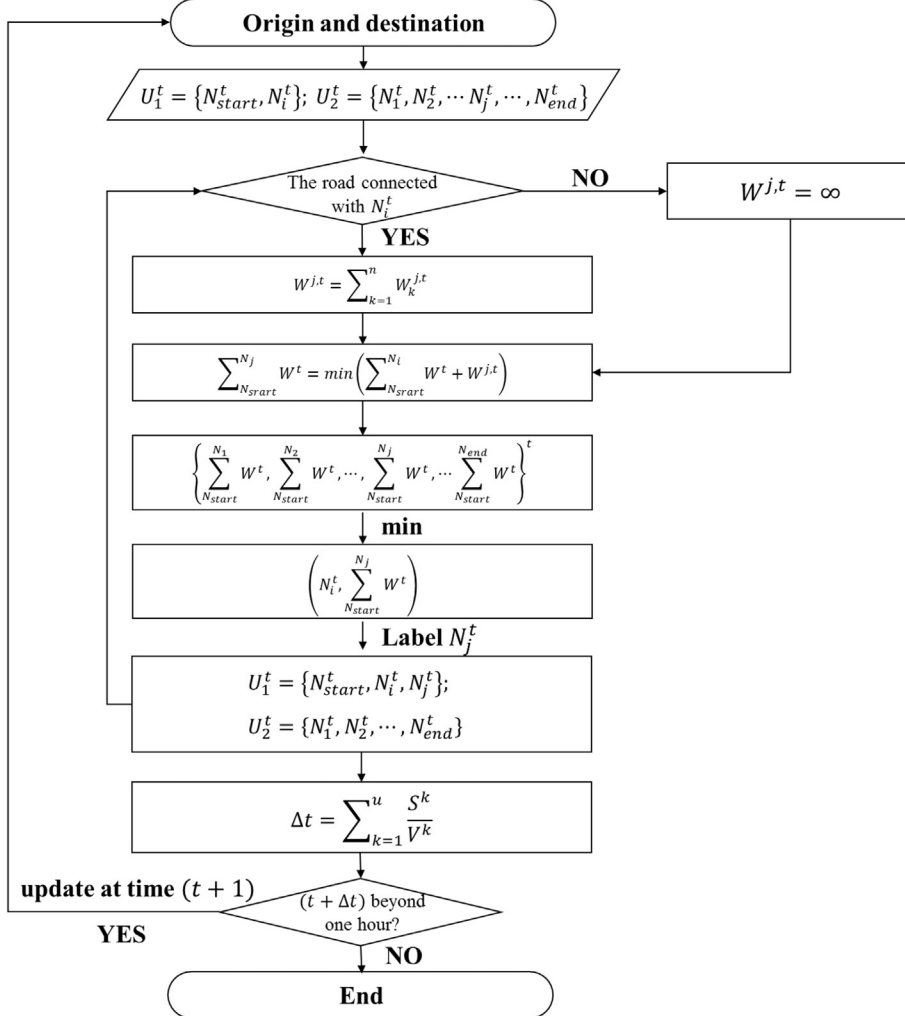
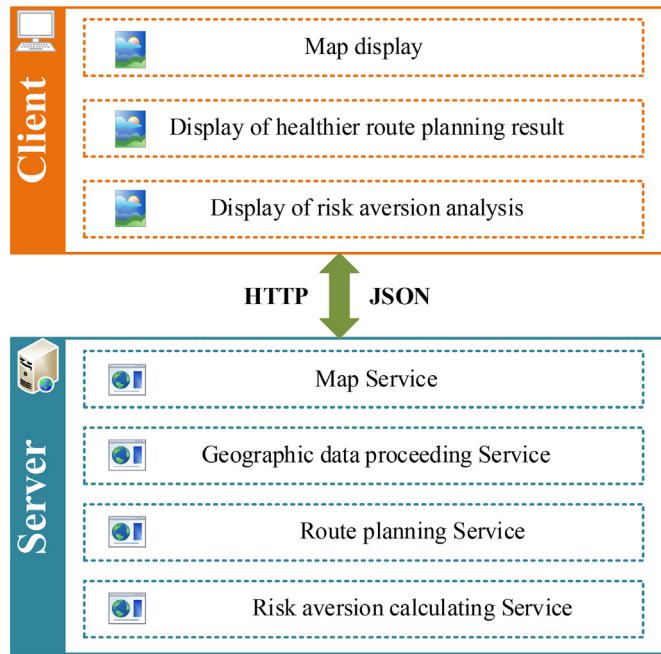


Fig. 2. The flowchart of dynamic Dijkstra route search method.



**Fig. 3.** Technical architecture of the HRP APP.

will be re-identified as a new healthier route by using the current location of the traveling person as the new start vertex. And the lowest risk weight of APE for all the new candidate roads are recalculated according to the updated surface map of air pollutant concentrations at the above certain time instant.

#### 2.4. Experimental implementation of online HRP service

In addition, to verify the effectiveness of HRP of HRP method, the development of online application (i.e. APP) service could be an effective and efficient way. For the HRP APP, the main technology framework includes two parts: server and client (see Fig. 3). As the key component of the APP system, the sever side mainly includes map service, geographic data proceeding service and route planning service. With the support of these web services, the server side could successfully execute the HRP method based on the inputs of near real-time air quality and associated data, and consequently respond the client request of healthier route search at any moment. Relatively, the client side is simple, only includes functions of users' request inputs and results display of healthier route search. All the requests and responses for HRP between server and client interact with HTTP and JSON techniques.

### 3. Case study

#### 3.1. Study area

Beijing-Tianjin-Hebei (BTH), the most economically and politically vibrant urban agglomeration in northeastern China, was selected for carrying out the performance test of proposed HRP method in this study (see Fig. 4).

#### 3.2. Data

##### 3.2.1. Air pollution data

Considering the air pollution based adverse health effects pointed out by the WHO, six critical outdoor air pollutants including PM<sub>2.5</sub>, PM<sub>10</sub>, SO<sub>2</sub>, CO, NO<sub>2</sub>, and O<sub>3</sub> were selected to more completely characterize health risk associated with APE. A total of 224 Hourly in situ

observations of these air pollutants from 17:00 and 19:00 on October 17, 2013 at 78 stationary monitoring sites (see Fig. 4) in the BTH region were collected from the China National Environmental Monitoring Centre (China Meteorological Data Service System, 2013) for this study.

##### 3.2.2. AOD data

As a parameter corresponding to the vertical path from Earth's surface to the top of atmosphere, AOD data has been widely utilized to estimate the ground concentrations of PM<sub>2.5</sub> and PM<sub>10</sub> (You, Zang, Zhang, et al., 2015; Ma, Wang, Yu, et al., 2016; Li, Zou, & Fang, 2019). For this study, the AOD raster data at 500-m spatial resolution were retrieved from the MODIS-Aqua images at the same date using the Simplified Aerosol Retrieval Algorithm (SARA) (Bilal, Nichol, Bleiweiss, et al., 2013).

##### 3.2.3. Land use/cover data

Generally, land use/cover data are considered the essential explanatory geographic factors for LUR/GWR based air pollution mapping (Briggs, Collins, Elliott, et al., 1997; Fang, Zou, & Liu, 2016). The data were collected from the national geographical condition monitoring databases of the BTH region in 2013. Categories of the original land use/cover raster data were reclassified as woodland, farmland, grassland, built-up, bareland and watershed (see Fig. 1), based on our previous experience in air pollution mapping in this area (Zou, Pu, et al., 2016).

##### 3.2.4. Road network and surface dust data

According to previous source apportionment findings in the BTH region, traffic and surface dust are also factors deteriorating local air quality (Zou, Pu, et al., 2016; Cheng, Lang, Zhou, et al., 2013; Žíková, Wang, Yang, et al., 2016). Because of the limited availability of data, we used all levels of road network and dust area in vector format as substitutes for real-time vehicle emissions and dust emissions. And these data were also acquired from the national geographical condition monitoring databases of the BTH region in 2013. Meanwhile, the speed limit and the congestion status of each road were also collected (<http://lbs.amap.com>). With these data, the APE risk (i.e. adverse health effects) could be quantitatively calculated for any person traveling on a certain road.

##### 3.2.5. Meteorological data

Meteorological factors greatly affect the dispersion of air pollutants. Based on previous findings in the BTH region (Zou, Pu, et al., 2016), hourly average temperature, relative humidity, atmospheric pressure, precipitation, wind speed and direction for the study time period mentioned above were all collected. In this process, these meteorological parameters from China Meteorological Data Service System (2013) were interpolated as grid based continuous surfaces by using the nearest-neighbor sampling strategy to make them available at the stationary monitoring sites Table 2

### 3.3. Results

#### 3.3.1. Spatial pattern of air pollutants concentrations

Fig. 5 illustrates the grid-based concentrations of six air pollutants at 500 m spatial resolution produced by LUR models with an acceptable accuracy (i.e. the adjusted R<sup>2</sup> is 0.39–0.67 and the RMSE is 0.42–27 µg/m<sup>3</sup>) in the experimental time period (i.e., 17:00–18:00, 18:00–19:00, 19:00–20:00). It can be found that the hourly concentrations of PM<sub>2.5</sub>, PM<sub>10</sub> and NO<sub>2</sub> are clearly higher than the acceptable safety thresholds of China's national air quality standards (CNAQS) in some parts of the BTH region with maximum values at 296 µg/m<sup>3</sup>, 411 µg/m<sup>3</sup> and 405 µg/m<sup>3</sup> respectively, while those of SO<sub>2</sub>, O<sub>3</sub> and CO in the entire BTH region are almost close to or lower than the standard thresholds 190 µg/m<sup>3</sup>, 148 µg/m<sup>3</sup> and 10 mg/m<sup>3</sup>, respectively. Meanwhile, internal comparisons of concentration maps for each air pollutant at

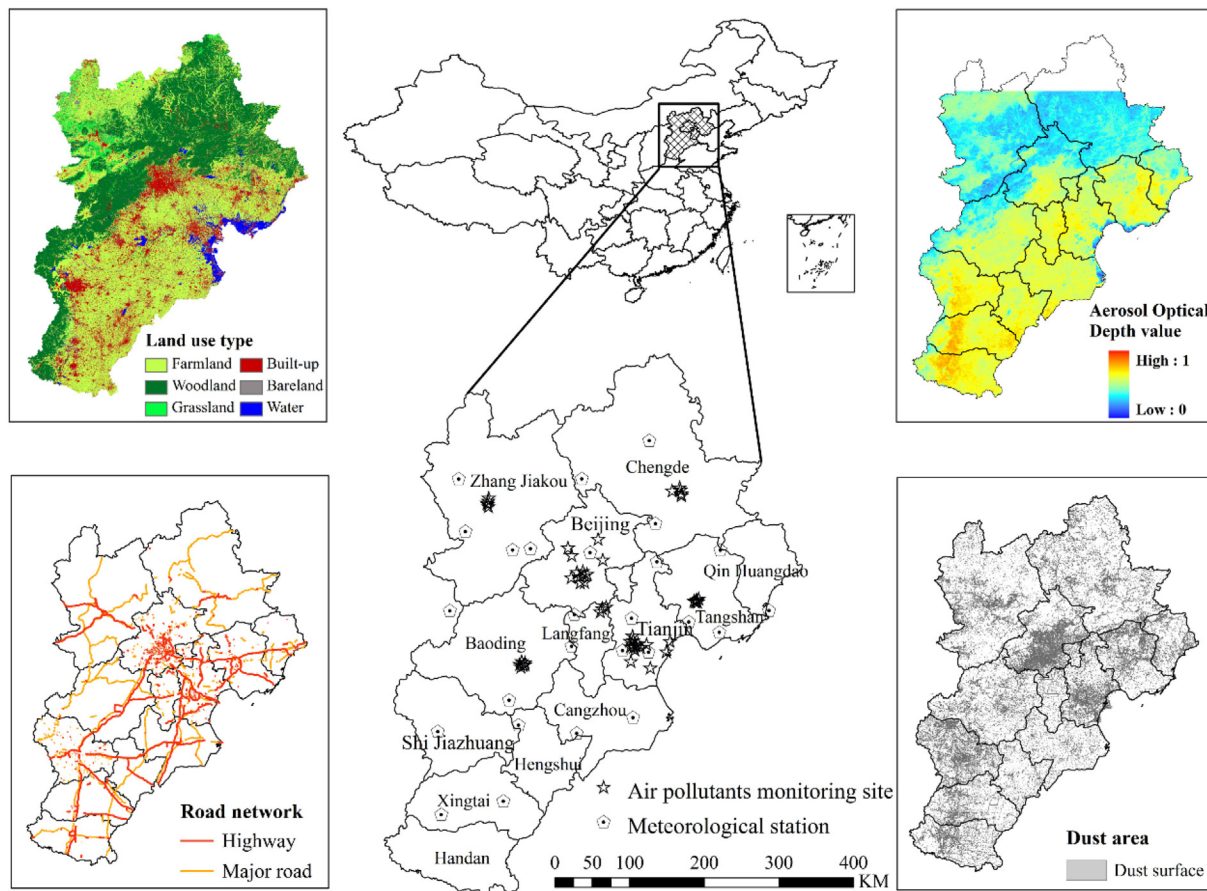


Fig. 4. Study area and data.

different times further reveal that air pollution concentration indeed varies over the time and across the study region. Furthermore, while large variations of  $\text{PM}_{2.5}$  and  $\text{PM}_{10}$  are especially obvious in southwestern Hebei province, those relatively slight changes of  $\text{O}_3$  and  $\text{NO}_2$

are mainly located in Beijing city.

### 3.3.2. Grid-based APE risk surfaces

Fig. 6 shows are the grid-based exposure risk surfaces in the BTH

**Table 2**  
Details of initialized predictors for each type of data.

Category	Variables	Unit	Spatial scale	Positive/ Negative effect	Description
Air pollutants	$\text{PM}_{2.5}$	$\mu\text{g}/\text{m}^3$	N/A	N/A	Hourly ground-level measurements which is the dependent variable.
	$\text{PM}_{10}$	$\mu\text{g}/\text{m}^3$			
	$\text{SO}_2$	$\mu\text{g}/\text{m}^3$			
	$\text{NO}_2$	$\mu\text{g}/\text{m}^3$			
	$\text{O}_3$	$\mu\text{g}/\text{m}^3$			
	CO	$\mu\text{g}/\text{m}^3$			
Satellite data	AOD	N/A	1 km	Positive	Aerosol optical depth which is related to the fine particles in the atmospheric column.
Road network and surface dust data	Road <sub>Len</sub>	m	50, 60, 70, 80, 90, 100, 150, 200, 250, 300, 350, 400, 450, 500, 1000, 1500, 2000, 2500, 3000, 3500, 4000, 4500, 5000 m	Positive	Total road length, the distance from road and dust area percentage in specific buffer radius which can represent the effects of traffic and dust emission on air pollutants concentrations.
Land use/cover data	Dust <sub>perc</sub>	%			
	Building <sub>perc</sub>	%	100, 200, 300, 400, 500, 1000, 1500, 2000, 2500, 3000, 3500, 4000, 4500, 5000 m	Positive	Original land use/cover data has been reclassify into woodland, farmland, grassland, building, bareland, and watershed six types, which can reflect the air pollutants' emissions.
	Woodland <sub>perc</sub>	%		Negative	
	Bareland <sub>perc</sub>	%		Negative	
	Grassland <sub>perc</sub>	%		Negative	
	Farmland <sub>perc</sub>	%		Negative	
Meteorological data	Watershed <sub>perc</sub>	%		Negative	
	WS	$\text{m}/\text{s}$	N/A	Negative	Meteorological data, including wind speed (WS), precipitation (PE), relative humidity (RH), hourly average temperature (Temp), and pressure (PS), can influence the dispersion of air pollutants.
	PE	mm	N/A	Negative	
	RH	%	N/A	Positive	
	Temp	K	N/A	Negative	
	PS	hPa	N/A	Positive	

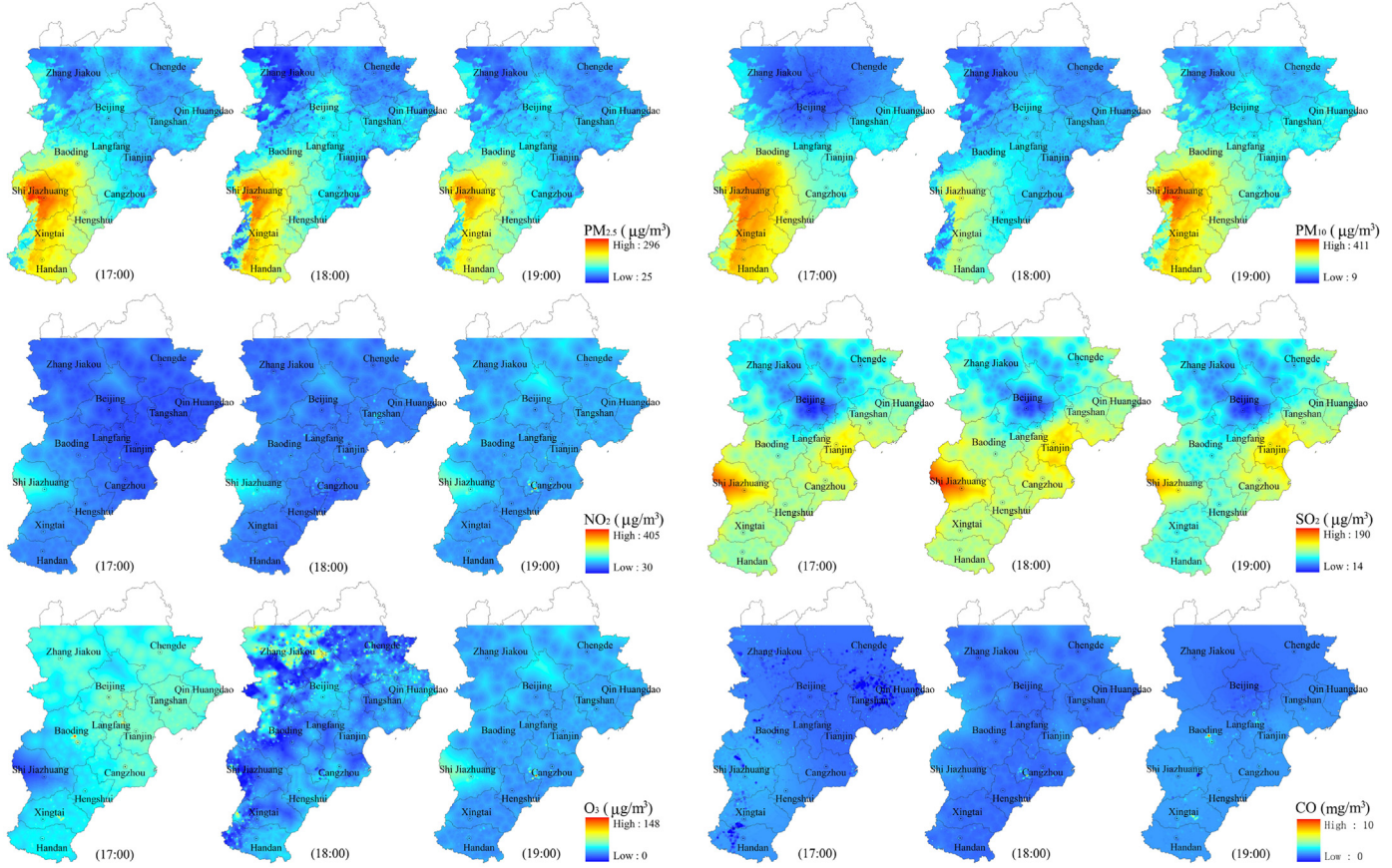


**Fig. 5.** Example maps showing concentration of different air pollutants at experiment time window.

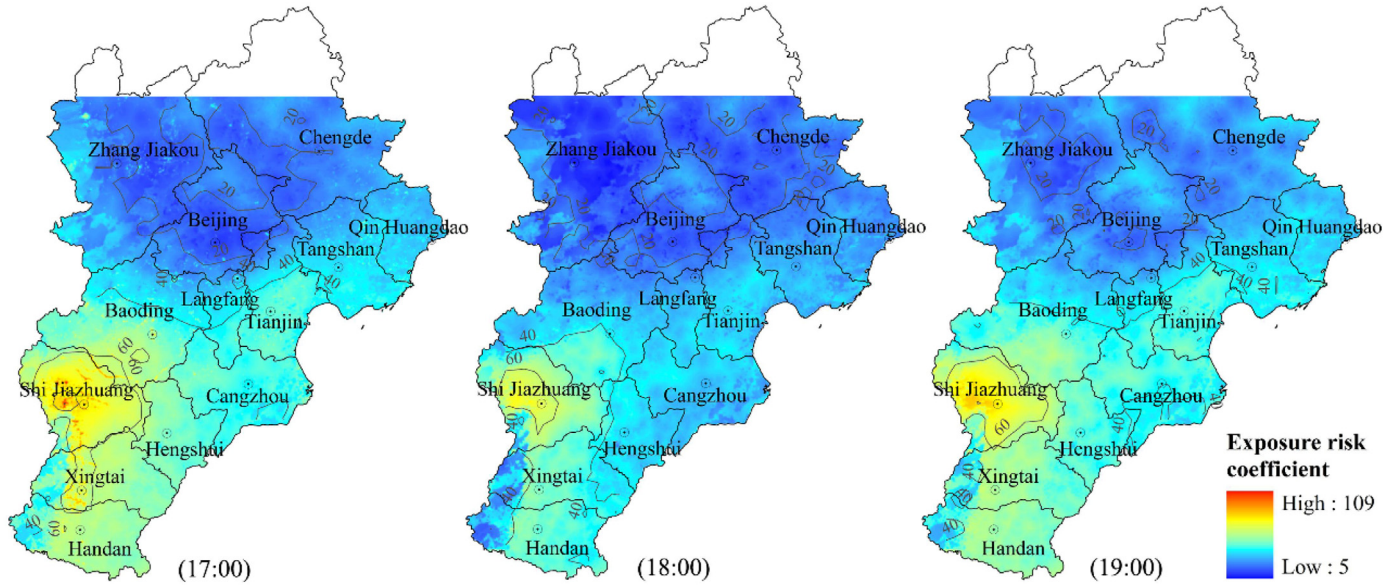


**Fig. 6.** Example grid-based exposure risk surfaces in the BTH region.

region at three different times (i.e., 17:00, 18:00, and 19:00). As shown in Fig. 7, there is obvious spatial heterogeneity for the exposure risk coefficients (i.e. ranging from 5 to 109) with lower risk mainly widely spreading in the northern area, higher risk concentrating on the southwestern area, and the median ones covering the central and eastern parts of the BTH region. The lower risk area (e.g. Beijing, Zhangjiakou) has generally an exposure risk coefficient at a value of no > 20, while those exposure risk coefficient values are 40 for median

(e.g. Baoding) and 60 for higher risk areas (e.g. Handan), respectively. Cities like Shijiazhuang and Xingtai experienced the highest exposure risk with coefficient values > 80.

Meanwhile, comparisons of the exposure risk surfaces at different times clearly display that areas with the highest exposure risk (i.e., risk coefficient values great than 80) always located in the Shijiazhuang city over the entire experimental time period. While the areas with relatively lower exposure risk (i.e., risk coefficient values between 60 and

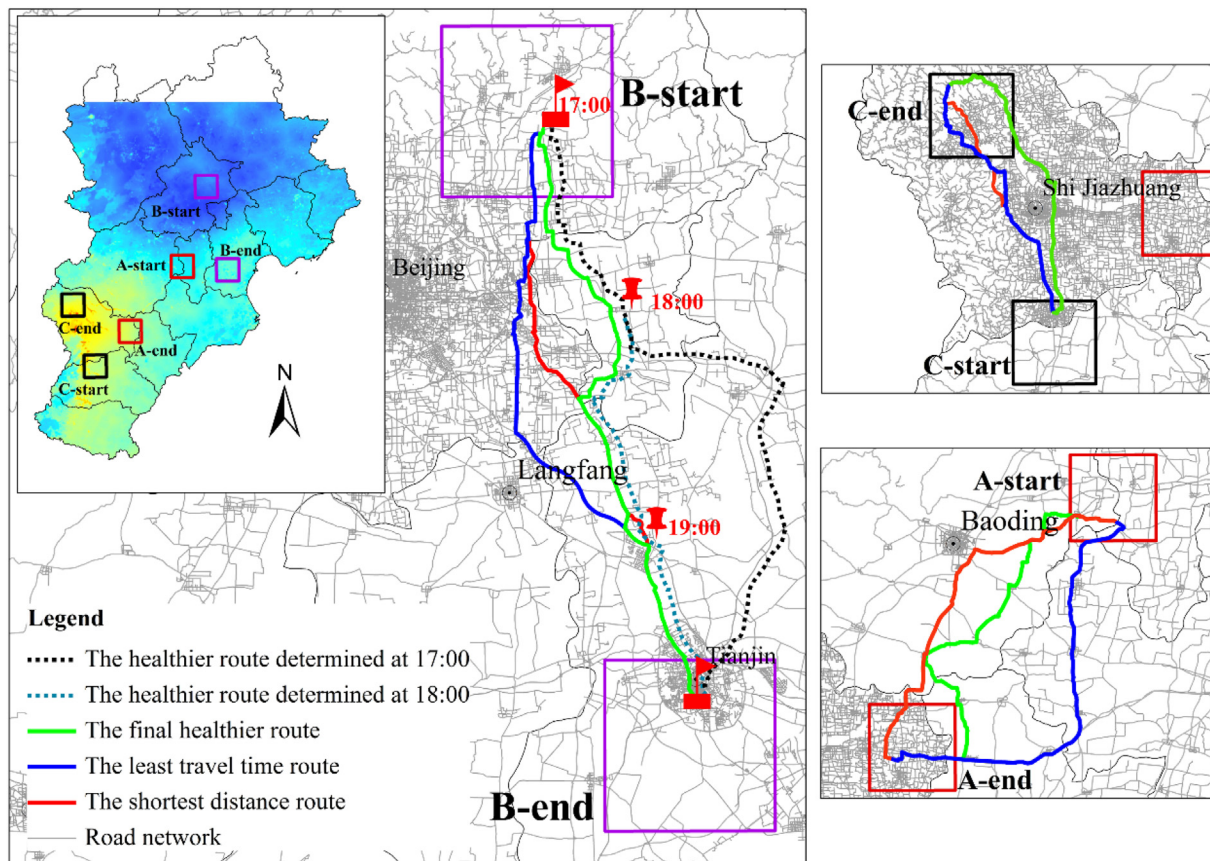


Fig. 7. Example healthier routes identified by the HRP method.

80) shrank from Xingtai and Handan at 17:00 pm to the surrounding area of Shijiazhuang city at 18:00 pm, this type of area again expanded at 19:00 pm to have an exposure risk pattern almost identical to the one at 17:00 pm. Similarly, this variation did occur for areas with median exposure risk mainly clustered in the eastern and central BTH region including Tianjin municipality and cities of Qinhuangdao, Tangshan, Baoding, Langfang, Cangzhou, Hengshui. For other areas with even lower exposure risk, changes of risk coefficients during 17:00 pm to 19:00 pm relatively remained stable.

### 3.3.3. Healthier routes with the lowest APE risk

Fig. 7 shows the search results of healthier routes (i.e., Green line) for various air pollution scenarios (i.e., Group 1: A-start and A-end regions with wide exposure risk variation, Group 2: B-start and B-end regions with low exposure risks and insignificant exposure risk variation, and Group 3: C-start and C-end regions with high exposure risks and insignificant exposure risk variation). While the Red line represents the shortest distance route, the Blue line indicates the least travel time route. Comparisons of these three types of color lines (i.e., Green, Red, and Blue lines) show that the spatial distribution of healthier routes is obviously different from the other two types of routes. Moreover, the routes determined by HRP method always kept updating values of conditions from 17:00 to 20:00 pm. In this process, the APE risk of a road segment (i.e., 26.07) at certain time T (e.g., 19:00–20:00) for the healthier routes exceeded that of least travel time route (i.e., 15.64) (see Table 3).

In addition, Table 3 further demonstrates that the Mean APE risk for healthier routes were always the lowest (i.e., A-start and A-end regions: 83.59, B-start and B-end regions: 74.83, and C-start and C-end regions: 163.38) in this case, although the healthier route might take longer time to travel and its length might not be the shortest. Compared to those of the shortest distance routes (i.e., A-start and A-end regions:

106.36, B-start and B-end regions: 88.27, and C-start and C-end regions: 174.23), the corresponding APE risk of health routes are 27.24%, 17.96%, and 6.64% lower, respectively. Generally, for regions with insignificant variations of APE risks (e.g., regions between B-start and B-end and regions between C-start and C-end), there was no remarkable difference between the APE risk values associated the healthier routes and the least travel time routes (i.e., the Bias L-H for regions between B-start and B-end is 0.13% and the Bias L-H for regions between C-start and C-end is 0.86%). However, a complete reversal occurred in regions with wide exposure risk variations (i.e., A-start and A-end regions), the difference in the APE risk values between the healthier routes and the least travel time routes reached 21.38%.

### 3.3.4. Experimental online HRP APP service

The online HRP app service include two main functional inferences: origin/destination (O/D) input and route search, result display. O/D input and route search function could display the city background geo-environment, road network, users' locations, and provides a window for users to input the O/D points healthier routes searched. In this process, locations of users could be automatically positioned and loaded in real time. The result display function includes four sub-inferences: healthier route (Fig. 8 (a)), least travel time route (Fig. 8 (b)), shortest distance route (Fig. 8 (c)) and risk aversion analysis (Fig. 8 (d)). This function can provide visual inferences for users to look over any road segment's detail information about exposure risk values, distance lengths and travel time and make the final travel decision based on the risk aversion analysis.

Additionally, Jmeter is used as a tool to test the performance of the service, and the test indicators are response time and throughput. Table 4 shows the results of performance test. When the number of users is < 15, the response time of HRP increases linearly with the number of users. For each additional user, the response time delay is

**Table 3**

Quantitative comparison of the mean APE risk from HRP and traditional methods for route search.

Regions*	Time interval	The shortest distance route			The least travel time route			The healthier route			Difference S-H	Difference L-H
		Mean distance (km)	Mean time (minute)	Mean APE risk	Mean distance (km)	Mean time (minute)	Mean APE risk	Mean distance (km)	Mean time (minute)	Mean APE risk		
From A-start region to A-end region	17–18	69	60	36.76	94	60	44.07	78	60	30.58	20.21%	44.11%
	18–19	67	60	38.91	72	60	41.75	73	60	26.94	44.43%	54.97%
	19–20	37	38	30.69	18	19	15.64	50	43	26.07	17.72%	–40.01%
<b>Sum</b>	<b>17–20</b>	<b>173</b>	<b>158</b>	<b>106.36</b>	<b>184</b>	<b>139</b>	<b>101.46</b>	<b>201</b>	<b>163</b>	<b>83.59</b>	<b>27.24%</b>	<b>21.38%</b>
From B-start region to B-end region	17–18	53	60	15.87	56	60	15.90	61	60	15.26	4.00%	4.19%
	18–19	54	60	23.81	68	60	25.45	70	60	24.79	–3.95%	2.66%
	19–20	62	69	48.59	55	47	33.58	62	51	34.78	39.71%	–3.45%
<b>Sum</b>	<b>17–20</b>	<b>169</b>	<b>189</b>	<b>88.27</b>	<b>179</b>	<b>167</b>	<b>74.93</b>	<b>193</b>	<b>171</b>	<b>74.83</b>	<b>17.96%</b>	<b>0.13%</b>
From C-start region to C-end region	17–18	54	60	73.42	56	60	73.96	55	60	71.57	2.58%	3.34%
	18–19	55	60	62.97	62	60	63.49	62	60	63.66	–1.08%	–0.27%
	19–20	42	39	37.84	36	29	27.33	37	30	28.15	34.42%	–2.91%
<b>Sum</b>	<b>17–20</b>	<b>151</b>	<b>159</b>	<b>174.23</b>	<b>154</b>	<b>149</b>	<b>164.78</b>	<b>154</b>	<b>150</b>	<b>163.38</b>	<b>6.64%</b>	<b>0.86%</b>

Note: \*means there are 10 selected routes between each pair of regions. Difference S-H = (Mean APE for shortest distance route - Mean APE for healthier route) × 100%/ Mean APE for healthier route; Difference S-H = (Mean APE for least travel time route - Mean APE for healthier route) × 100%/ Mean APE for healthier route. The words in bold mean the total values of each test region.

about 70 ms, and the throughput increases sharply. When the number of users is 15–80, the response time increases rapidly and the throughput remains stable, about 13.0/s, and when the number of users is 40, The maximum throughput is 13.5/s, and the corresponding response time is 2999 ms. When the number of users is > 40, the system throughput increases and decreases, and the average response time also increases rapidly.

#### 4. Discussion

By integrating techniques of fine scale air pollution mapping, on-road health risk estimation, and dynamic Dijkstra algorithm-based route search, we proposed an innovative HRP method for healthier route planning and consequently for personal exposure risk minimizing in this study. As a new development of route search algorithm, the theoretical and practical advantages and limitations of HRP should be cautiously noted before widespread implementation.

Theoretically, HRP represents a new framework as it for the first time introduces fine-scale air pollution maps and exposure-response

parameters into the route search field. With this theoretical framework, the computation of on-road potential adverse health effects caused by air pollution was realized, rather than the estimation of exposure intensity as reported so far (Ezzati & Kammen, 2001; Lelieveld et al., 2015). And this will definitely provide a new insight into the fields of environment, traffic and public health at the solutions to risk circumvention and adverse health effect associated contribution factors analysis.

By fusing the fine scale air pollution maps with PM<sub>2.5</sub> concentration-based exposure-response parameters, the HRP method estimated the APE risk (i.e., potential adverse health effect) of each road segment for the entire road network caused by PM<sub>2.5</sub> in the urban area of BTB. The differences among the APE risk surfaces (i.e., Fig. 6) and air pollutant concentration maps (i.e., Fig. 5), as well as the spatial heterogeneity confirmed the necessity of APE risk weight calculation for the entire road network. Compared to previous methods assessing air pollution exposure (Sharker & Karimi, 2014; Zou, Wilson, Zhan, et al., 2009), the APE risk estimated under the HRP framework takes into account the potentially real exposure-response relationship rather than using the

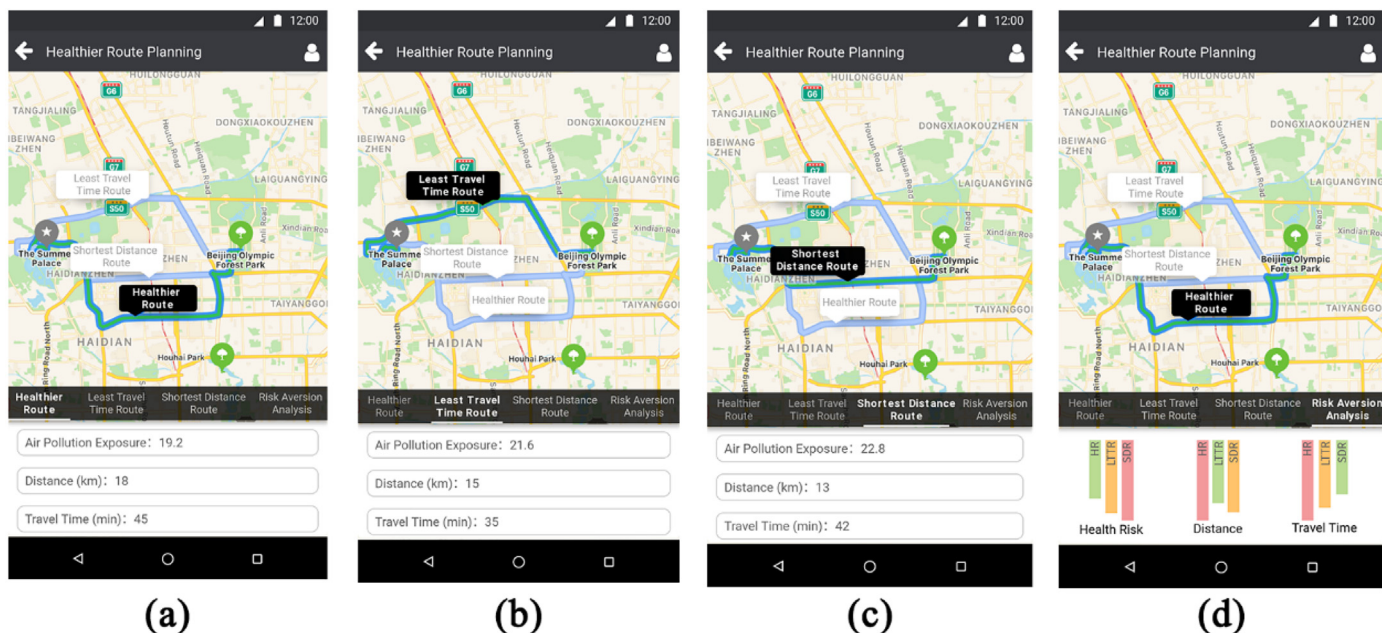


Fig. 8. Main functional interfaces of HRP APP.

**Table 4**

Performance test results of HRP online APP.

Number of concurrent requests	Total number of requests	Average response time(ms)	95% Line	99% Line	Error(%)	Throughput(/sec)
5	2000	406	546	1411	0%	11.3
10	2000	770	941	1675	0%	12.7
16	2000	1185	1362	2105	0%	13.0
20	2000	1508	1880	2642	0%	13.1
25	2000	1866	2121	2818	0%	13.2
40	2000	2999	3415	4065	0%	13.4
50	2000	3724	4364	5939	0%	13.1
80	2000	6015	7289	8145	0%	12.9
100	2000	7586	9120	9542	0%	12.7
125	2000	10,028	13,042	13,759	0%	12.0

population weighted concentration (Bell, Ebisu, Leaderer, et al., 2014) or AQI (Sharker & Karimi, 2014) as alternatives of adverse health effects. However, the implementation of exposure risk estimation might need to be extended in studies that involve other pollutants such as: polycyclic aromatic hydrocarbon (PAHs) and volatile organic compounds (VOC), once the data were available. Moreover, although the exposure-response parameter ‘mortality rate’ in this study provided a possible solution to quantifying the adverse health effects from air pollutants, more specific parameters such as ‘incidence of a certain disease’ need to be comprehensively calibrated for various susceptible population if we would like to develop a personally customized healthier route search method. Additionally, the forecasting of hourly fine resolution air pollutant mapping necessary for the HRP method when the distance is long (Xu et al., 2018).

Based on the dynamic Dijkstra algorithm with a mechanism for automatically updating values of APE risk, the HRP method were tested with hundreds of pairs of randomly selected origins and destinations over various air pollution scenarios in this study and the Table 3 showed the representative results. As illustrated, the on-road sum APE risks with healthier routes were lower than those with shortest distance routes and least travel-time routes for all the tests and varied with time. These results certainly verified the significance of the brand new HRP method in protecting human health through reducing exposure risk in daily traveling, even though it might result in longer travel distance or time occasionally. And this actually broadened the options for public travel routes.

However, the healthier route determined by the HRP method sometimes similar with shortest distance route or least travel time route. When there is only the unique choice of route from location A to location B, the healthier route, shortest route and least travel time route are the same. Meanwhile, when the spatial distribution of air pollution is relatively homogeneous, the healthier route and shortest route are also with small difference. In this situation, the exposure time might be the leading factor influencing the quantity of exposure risk compared to the spatially light difference of air pollution concentrations. And this actually implies that the merit of HRP method would be better embodied in areas with obviously internal heterogeneity of air pollution. With the development of urban road network, stereo-traffic traveling including ground (i.e., driving, bicycling, or walking) and underground (i.e., taking subway) is becoming popular, variations of air pollution concentrations among these 3-dimensional space with different sources and dispersion conditions will inevitably increase. These variations could be accurately captured with the maturity of air quality monitoring network. As a result, community-based finer scale air pollution mapping and associated exposure risk estimation would be achievable.

In summary, as a new method, the HRP performed well in searching the healthier routes based on results from the case study. However, more efforts are needed for future improvements and implementation of HRP. Except for the construction of the stereo in situ monitoring network for air quality and the development of the typically targeted exposure-response parameters, spatiotemporally depended ratios of

indoor/outdoor air pollution exposure, efficiency of route search algorithms, further systemic performance test with real-life dataset, as well as the release of industrial policies for widespread application should also be considered. And these systematical works might possibly lead to the boost of research in field of real-time assessment fine scale of APE risk.

## 5. Conclusion

Aiming at reducing adverse health effects caused by air pollution exposure during daily travel in large urban areas, this study for the first time proposes a near real-time healthier route search method to minimize public APE risk. Compared to the traditional route search algorithms reported in the literatures, this method provides a new theoretical framework for searching out the APE risk based healthier route by introducing the exposure-response relationship, rather than simply considering the distance length, journey time, or the exposure intensity. Moreover, using the urban area of BTB as a case, evaluations confirmed that the proposed HRP method can effectively identify routes with lower APE risk. And this risk mitigation effect is especially significant in areas with wide exposure risk variations over space and time. Therefore, in metropolis with increasing travel distance, journey time, as well as the heterogeneous distribution of air pollution in urban sprawl, the role of HRP method in reducing public APE risk could be more important. It can be utilized as one of the promising ways to protect human health through planning the healthier routes during daily travel.

## Acknowledgements

This work was supported by the National Key Research and Development Program of China [grant number 2016YFC0206205 and 2016YFC0206201]; the National Natural Science Foundation of China [grant number 41871317]; the Innovation Driven Program of Central South University [grant number 2018CX016].

## References

- Airnow Website (2015). <http://airnow.gov/index.cfm?action=aqibasics.aqi>.
- Alexiou, D., & Katsavounis, S. (2015). A multi-objective transportation routing problem. *Operational Research*, 15(2), 199–211. <https://doi.org/10.1007/s12351-015-0173-1>.
- Bell, M. L., Ebisu, K., Leaderer, B. P., et al. (2014). Associations of PM<sub>2.5</sub> constituents and sources with hospital admissions: Analysis of four counties in Connecticut and Massachusetts (USA) for persons ≥ 65 years of age. *Environmental Health Perspectives*, 122(2), 138–144. <https://doi.org/10.1289/ehp.1306656>.
- Bigazzi, A. Y., & Figliozi, M. A. (2015). Roadway determinants of bicyclist exposure to volatile organic compounds and carbon monoxide. *Transportation Research Part D: Transport and Environment*, 41, 13–23. <https://doi.org/10.1016/j.trd.2015.09.008>.
- Bilal, M., Nichol, J. E., Bleiweiss, M. P., et al. (2013). A Simplified high resolution MODIS Aerosol Retrieval Algorithm (SARA) for use over mixed surfaces. *Remote Sensing of Environment*, 136, 135–145. <https://doi.org/10.1016/j.rse.2013.04.014>.
- Briggs, D. J., Collins, S., Elliott, P., et al. (1997). Mapping urban air pollution using GIS: A regression-based approach. *International Journal of Geographical Information Science*, 11(7), 699–718. <https://doi.org/10.1080/136588197242158>.
- Cheng, S., Lang, J., Zhou, Y., et al. (2013). A new monitoring-simulation-source apportionment approach for investigating the vehicular emission contribution to the PM<sub>2.5</sub>

- pollution in Beijing, China. *Atmospheric Environment*, 79, 308–316. <https://doi.org/10.1016/j.atmosenv.2013.06.043>.
- China Meteorological Data Service System (2013). <http://data.cma.cn/>.
- Choi, Y., Kang, D., & Bahk, S. (2014). Improvement of AODV routing protocol through dynamic route change using hello message. *International Conference on Information and Communication Technology Convergence (ICTC), October 22–24 2014 Busan* (pp. 117–121). . <https://doi.org/10.1109/ICTC.2014.6983096>.
- Defranco, E., Hall, E., Hossain, M., et al. (2015). Air pollution and stillbirth risk: Exposure to airborne particulate matter during pregnancy is associated with fetal death. *PLoS One*, 10(3), e0120594. <https://doi.org/10.1371/journal.pone.0120594>.
- Dijkstra, E. W. (1959). A note on two problems in connexion with graphs. *Numerische Mathematik*, 1(1), 269–271. <https://doi.org/10.1007/BF01386390>.
- Ezzati, M., & Kammen, D. M. (2001). Quantifying the effects of exposure to indoor air pollution from biomass combustion on acute respiratory infections in developing countries. *Environmental Health Perspectives*, 109(5), 481–488. <https://doi.org/10.2307/3454706>.
- Faiz, A. S., Rhoads, G. G., Demissie, K., et al. (2012). Ambient air pollution and the risk of stillbirth. *American Journal of Epidemiology*, 176(4), 308–316. <https://doi.org/10.1093/aje/kws029>.
- Fang, X., Zou, B., Liu, X., et al. (2016). Satellite-based ground PM<sub>2.5</sub> estimation using timely structure adaptive modeling. *Remote Sensing of Environment*, 186, 152–163. <https://doi.org/10.1016/j.rse.2016.08.027>.
- Franklin, M., Zeke, A., & Schwartz, J. (2007). Association between PM<sub>2.5</sub> and all-cause and specific-cause mortality in 27 US communities. *Journal of Exposure Science & Environmental Epidemiology*, 17(3), 279–287. <https://doi.org/10.1038/sj.jes.7500530>.
- Fu, X., & Lam, W. H. (2014). A network equilibrium approach for modelling activity-travel pattern scheduling problems in multi-modal transit networks with uncertainty. *Transportation*, 41(1), 37–55. <https://doi.org/10.1007/s11116-013-9470-9>.
- George, B., & Kim, S. (2013). *Shortest path algorithms for a fixed start time. Spatio-temporal Networks: Modeling and Algorithms*. New York, NY: Springer New York25–43. [https://doi.org/10.1007/978-1-4614-4918-8\\_3](https://doi.org/10.1007/978-1-4614-4918-8_3).
- Guarnieri, M., & Balmes, J. R. (2014). Outdoor air pollution and asthma. *The Lancet*, 383(9928), 1581–1592. [https://doi.org/10.1016/S0140-6736\(14\)60617-6](https://doi.org/10.1016/S0140-6736(14)60617-6).
- Hajat, S., Armstrong, B., Wilkinson, P., et al. (2007). Outdoor air pollution and infant mortality: Analysis of daily time-series data in 10 English cities. *Journal of Epidemiology and Community Health*, 61(8), 719–722. <https://doi.org/10.1136/jech.2006.053942>.
- Hoek, G., Beelen, R., Hoogh, K. D., et al. (2008). A review of land-use regression models to assess spatial variation of outdoor air pollution. *Atmospheric Environment*, 42(33), 7561–7578. <https://doi.org/10.1016/j.atmosenv.2008.05.057>.
- Hynes, M. (2013). *Mobility matters:Technology, telework, and the (un) sustainable consumption of distance*. PhD Dissertation (PhD): National University of Ireland.
- Jerrett, M., Arain, A., Kanaroglou, P., et al. (2005). A review and evaluation of intraurban air pollution exposure models. *Journal of Exposure Science & Environmental Epidemiology*, 15(2), 185–204. <https://doi.org/10.1038/sj.je.7500388>.
- Jerrett, M., Arain, M. A., Kanaroglou, P., et al. (2007). Modeling the intraurban variability of ambient traffic pollution in Toronto, Canada. *Journal of Toxicology and Environmental Health, Part A*, 70(3–4), 200–212. <https://doi.org/10.1080/15287390600883018>.
- Johnson, M., Isakov, V., Touma, J. S., et al. (2010). Evaluation of land-use regression models used to predict air quality concentrations in an urban area. *Atmospheric Environment*, 44(30), 3660–3668. <https://doi.org/10.1016/j.atmosenv.2010.06.041>.
- Lai, H. K., Tsang, H., & Wong, C. M. (2013). Meta-analysis of adverse health effects due to air pollution in Chinese populations. *BMC Public Health*, 13(1), 360. <https://doi.org/10.1186/1471-2458-13-360>.
- Lelieveld, J., Evans, J. S., Fnais, M., et al. (2015). A. the contribution of outdoor air pollution sources to premature mortality on a global scale. *Nature*, 525(7569), 367–371. <https://doi.org/10.1038/nature15371>.
- Li, S., Zou, B., Fang, X., et al. (2019). Time series modeling of PM<sub>2.5</sub> concentrations with residual variance constraint in eastern mainland China during 2013–2017. *Science of the Total Environment*. <https://doi.org/10.1016/j.scitotenv.2019.135755>.
- Lu, F., Xu, D., Cheng, Y., et al. (2015). Systematic review and meta-analysis of the adverse health effects of ambient PM<sub>2.5</sub> and PM<sub>10</sub> pollution in the Chinese population. *Environmental Research*, 136, 196–204. <https://doi.org/10.1016/j.envres.2014.06.029>.
- Ma, X., Wang, J., Yu, F., et al. (2016). Can MODIS AOD be employed to derive PM<sub>2.5</sub> in Beijing-Tianjin-Hebei over China? *Atmospheric Research*, 181, 250–256. <https://doi.org/10.1016/j.atmosres.2016.06.018>.
- Mainali, M. K., Mabu, S., Yu, S., et al. (2011). Dynamic optimal route search algorithm for car navigation systems with preferences by dynamic programming. *IIEEE Transactions on Electrical and Electronic Engineering*, 6(1), 14–22. <https://doi.org/10.1002/tee.20601>.
- Möller, A., & Lindley, S. (2015). Influence of walking route choice on primary school children's exposure to air pollution-A proof of concept study using simulation. *Science of the Total Environment*, 530–532, 257–262. <https://doi.org/10.1016/j.scitotenv.2015.05.118>.
- Olvera, H. A., Garcia, M., Li, W., et al. (2012). Principal component analysis optimization of a PM<sub>2.5</sub> land use regression model with small monitoring network. *The Science of the Total Environment*, 425, 27–34. <https://doi.org/10.1016/j.scitotenv.2012.02.068>.
- Paul, A. (2013). Reviewing the axial-line approach to capturing vehicular trip-makers' route-choice decisions with ground reality. *Transportation*, 40(3), 697–711. <https://doi.org/10.1007/s11116-012-9436-3>.
- Pillac, V., Gendreau, M., Guéret, et al. (2013). A review of dynamic vehicle routing problems. *European Journal of Operational Research*, 225(1), 1–11. <https://doi.org/10.1016/j.ejor.2012.08.015>.
- Pope, C. A., Burnett, R. T., Krewski, D., et al. (2009). Cardiovascular mortality and exposure to airborne fine particulate matter and cigarette smoke shape of the exposure-response relationship. *Circulation*, 120(11), 941–948. <https://doi.org/10.1161/CIRCULATIONAHA.109.857888>.
- Qian, Z. S., & Zhang, H. M. (2013). A hybrid route choice model for dynamic traffic assignment. *Networks and Spatial Economics*, 13(2), 183–203. <https://doi.org/10.1007/s11067-012-9177-z>.
- Rahmani, M., & Koutsopoulos, H. N. (2013). Path inference from sparse floating car data for urban networks. *Transportation Research Part C: Emerging Technologies*, 30, 41–54. <https://doi.org/10.1016/j.trc.2013.02.002>.
- Ramezani, M., & Geroliminis, N. (2012). On the estimation of arterial route travel time distribution with Markov chains. *Transportation Research Part B: Methodological*, 46(10), 1576–1590. <https://doi.org/10.1016/j.trb.2012.08.004>.
- Ritz, B., Wilhelm, M., & Zhao, Y. (2006). Air pollution and infant death in southern California, 1989–2000. *Pediatrics*, 118(2), 493–502. <https://doi.org/10.1016/j.trb.2012.08.004>.
- Schepers, P., Fishman, E., Beelen, R., et al. (2015). The mortality impact of bicycle paths and lanes related to physical activity, air pollution exposure and road safety. *Journal of Transport and Health*, 2(4), 460–473. <https://doi.org/10.1016/j.jth.2015.09.004>.
- Scott, W., Ryan, K., Aimee, D., et al. (2011). Traffic-related air pollution and acute changes in heart rate variability and respiratory function in urban cyclists. *Environmental Health Perspectives*, 119(10), 1373–1378. <https://doi.org/10.1289/ehp.1003321>.
- Shang, Y., Sun, Z., Cao, J., et al. (2013). Systematic review of Chinese studies of short-term exposure to air pollution and daily mortality. *Environment International*, 54, 100–111. <https://doi.org/10.1016/j.envint.2013.01.010>.
- Sharker, M. H., & Karimi, H. A. (2014). Computing least air pollution exposure routes. *International Journal of Geographical Information Science*, 28(2), 343–362. <https://doi.org/10.1080/13658816.2013.841317>.
- Stutzer, A., & Frey, B. S. (2008). Stress that Doesn't pay: The commuting paradox. *The Scandinavian Journal of Economics*, 110(2), 339–366. <https://doi.org/10.1111/j.1467-9442.2008.00542.x>.
- Wang, D. Q., Wang, B. Q., & Bai, Z. P. (2012). Meta-analysis of association between air fine particulate and daily mortality of residents [in Chinese]. *Journal of Environmental Health*, 29(6), 529–532. <https://doi.org/10.16241/j.cnki.1001-5914.2012.06.027>.
- Xu, S., Zou, B., Lin, Y., et al. (2019). Strategies of method selection for fine-scale PM<sub>2.5</sub> mapping in an intra-urban area using crowdsourced monitoring. *Atmospheric Measurement Techniques*, 12(5), 2933–2948. <https://doi.org/10.5194/amt-12-2933-2019>.
- Xu, S., Zou, B., Shafi, S., et al. (2018). A hybrid Grey-Markov/LUR model for PM<sub>10</sub> concentration prediction under future urban scenarios. *Atmospheric Environment*, 187, 401–409. <https://doi.org/10.1016/j.atmosenv.2018.06.014>.
- You, W., Zang, Z., Zhang, L., et al. (2015). Estimating ground-level PM<sub>10</sub> concentration in northwestern China using geographically weighted regression based on satellite AOD combined with CALIPSO and MODIS fire count. *Remote Sensing of Environment*, 168, 276–285. <https://doi.org/10.1016/j.rse.2015.07.020>.
- Zheng, S., & Kahn, M. E. (2013). Understanding China's urban pollution dynamics. *Journal of Economic Literature*, 51(3), 731–772. <https://doi.org/10.1257/jel.51.3.731>.
- Ziková, N., Wang, Y., Yang, F., et al. (2016). On the source contribution to Beijing PM<sub>2.5</sub> concentrations. *Atmospheric Environment*, 134, 84–95. <https://doi.org/10.1016/j.atmosenv.2016.03.047>.
- Zou, B., Luo, Y., Wan, N., et al. (2015). Performance comparison of LUR and OK in PM<sub>2.5</sub> concentration mapping:A multidimensional perspective. *Scientific Reports*, 5, 8698. <https://doi.org/10.1038/srep08698>.
- Zou, B., Pu, Q., Bilal, M., et al. (2016). High-resolution satellite mapping of fine particulates based on geographically weighted regression. *IEEE Geoscience and Remote Sensing Letters*, 13(4), 495–499. <https://doi.org/10.1109/LGRS.2016.2520480>.
- Zou, B., Wilson, J. G., Zhan, F. B., et al. (2009). An emission-weighted proximity model for air pollution exposure assessment. *Science of the Total Environment*, 407(17), 4939–4945. <https://doi.org/10.1016/j.scitotenv.2009.05.014>.
- Zou, B., You, J., Lin, Y., et al. (2019). Air pollution intervention and life-saving effect in China. *Environment International*. <https://doi.org/10.1016/j.envint.2018.10.045>.
- Zou, B., Zheng, Z., Wan, N., et al. (2016). An optimized spatial proximity model for fine particulate matter air pollution exposure assessment in areas of sparse monitoring. *International Journal of Geographical Information Science*, 30(4), 727–747. <https://doi.org/10.1080/13658816.2015.1095921>.